Evidence of the Griffiths phase in multiferroic $BiMnO_3$ and $BiFe_{0.5}Mn_{0.5}O_3$ films

V. G. Prokhorov[a] and G. G. Kaminsky

Institute of Metal Physics, NASU, Kiev 03142, Ukraine

J. M. Kim, Y. J. Yoo, and Y. P. Lee

q-Psi and Department of Physics, Hanyang University, Seoul 133-791, Korea

V. L. Svetchnikov

National Center for HREM, TU Delft 2628AL, The Netherlands

G. G. Levchenko, Yu. M. Nikolaenko, and V. A. Khokhlov

Donetsk Institute for Physics and Technology, NASU, Donetsk 83114, Ukraine
(Submitted December 15, 2011)
Fiz. Nizk. Temp. **38**, 531–537 (May 2012)

Microstructure and magnetic properties of $BiMnO_3$ and $BiFe_{0.5}Mn_{0.5}O_3$ films, prepared by rf magnetron sputtering on $LaAlO_3$ (001) single-crystalline substrate, are investigated. The selected-area electron diffraction analysis allows us to identify the crystal structure of the $BiMnO_3$ film as orthorhombic, while the $BiFe_{0.5}Mn_{0.5}O_3$ film has a hexagonal lattice symmetry. High-resolution electron microscopy study reveals the presence of strip-domain phase with a periodic spacing of about $3c$ in both films. Magnetic measurements show that in addition to the basic paramagnetic phase the films exhibit Griffiths phase behavior in a wide temperature range. We argue that the observed weak ferromagnetism is due to the strip-domain layered inclusions, rather than intrinsic physical origin of the films. © *2012 American Institute of Physics*. [http://dx.doi.org/10.1063/1.4709440]

1. Introduction

Multiferroics have attracted considerable attention due to their interesting fundamental science related to simultaneous effects of ferroelectric and magnetic ordering and their potential for applications in information storage, such as in spintronic devices and sensors. Bismuth ferrite and bismuth manganite, $BiFeO_3$ and $BiMnO_3$, are among the most studied single-component multiferroic compounds. The first of these is a canted G-type antiferromagnet (AFM) with Néel point $T_N \simeq 643$ K, ferroelectric transition temperature $T_C \simeq 1103$ K,[1–4] and a weak ferromagnetic (FM) moment ($\simeq 0.02\,\mu_B$/Fe),[5] arising from the antisymmetric Dzyaloshinskii–Moriya (DM) exchange.[6,7] At the same time, enhancement in the FM response is important because such an improvement can help utilize this compound for practical applications. From this standpoint, $BiMnO_3$ is more suitable due to the fact that FM ordering appears at $T_C \simeq 105$ K,[8] and ferroelectric polarization appears at $T_C \simeq 450$ K.[9–11] However, the measured ferroelectric effect for this compound is much smaller than that calculated from the first principle,[12] making it difficult to relate measured hysteresis loops to bulk ferroelectricity. Recent efforts in improvement of ferroelectric and ferromagnetic properties of the considered multiferroics are focused on preparation of $BiFeO_3$–$BiMnO_3$ alloy systems,[13–18] which are promising for practical implementation. On the other hand, the influence of crystal-lattice symmetry, microstructure topology, and accumulated lattice strain provided by epitaxial growth of the films, on the magnetic and ferroelectric properties of this multiferroic system has not been adequately studied.

In this paper we report experimental results for $BiMnO_3$ (BMO) and $BiFe_{0.5}Mn_{0.5}O_3$ (BFMO) films deposited on a $LaAlO_3$ (LAO) (001) single-crystalline substrate. Peculiarities of the crystal structure and magnetic behavior are discussed in detail.

2. Experimental techniques

The films were prepared by rf magnetron sputtering at substrate temperature of 650 °C.[19] To avoid the influence of lattice strain accumulated during deposition all films were annealed at 900 °C for 2 h in air. The thickness of the films was $d \simeq 160$ nm. High-resolution electron-microscopy (HREM) and electron-diffraction (ED) studies were carried out using a Philips CM300UTFEG microscope with a field emission gun operated at 300 kV. Point resolution of the microscope was on the order of 0.12 nm. All microstructure measurements were carried out at room temperature. Field-cooled (FC) and zero-field-cooled (ZFC) magnetization curves were obtained using a Quantum Design SQUID magnetometer for in-plane magnetic field orientation. To eliminate the influence of diamagnetic response from LAO, magnetization curves obtained for the bare substrates were subtracted from the raw experimental curves.[4]

3. Microstructure of the films

Figure 1 shows (a) the high-magnification cross-sectional HREM image and (b) the typical selected-area electron diffraction (SAED) pattern along the [010] zone axes for the BMO film. Since alternative SAED patterns were not observed one can conclude that the major phase of the BMO film has orthorhombic crystal structure with lattice parameters $a \simeq b \simeq 0.56$ nm, $c \simeq 0.7838$ nm, and $\alpha = \beta = \gamma \simeq 90°$, which are very close to the published results.[20,21] However, small regions of the long-periodic strip-domain phase, represented by the inset in Fig. 1(a), are found as well. In this

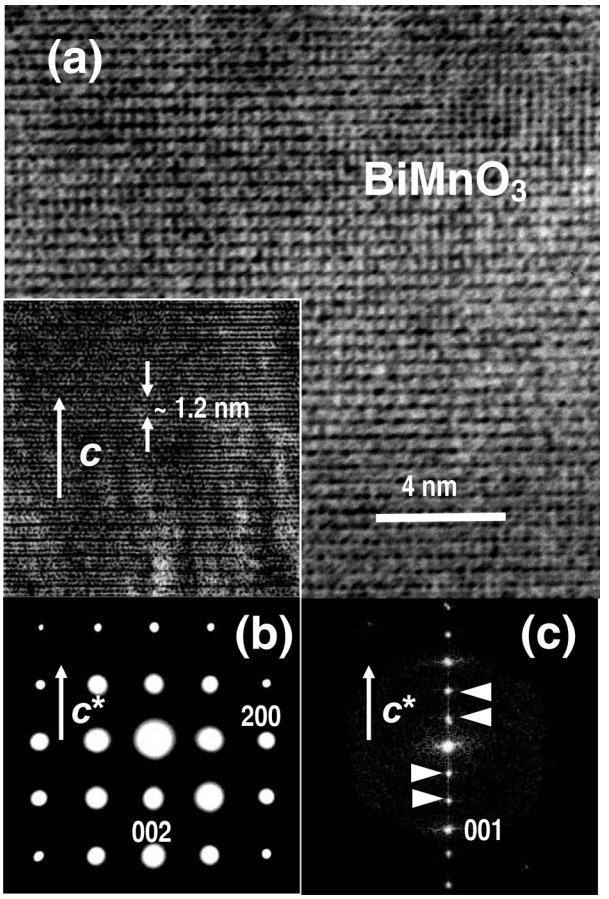

FIG. 1. (a) High-magnification cross-sectional HREM image for the BMO film. The inset presents the same image for the strip-domain phase. (b) The [010] zone-axis ED pattern for the basic orthorhombic film phase. (c) The FFT pattern of the HREM image, represented by the inset in *a*. White arrows show the period of strip- domains. The (001) spot indicates that the strip-domain phase has the crystal lattice of the basic phase.

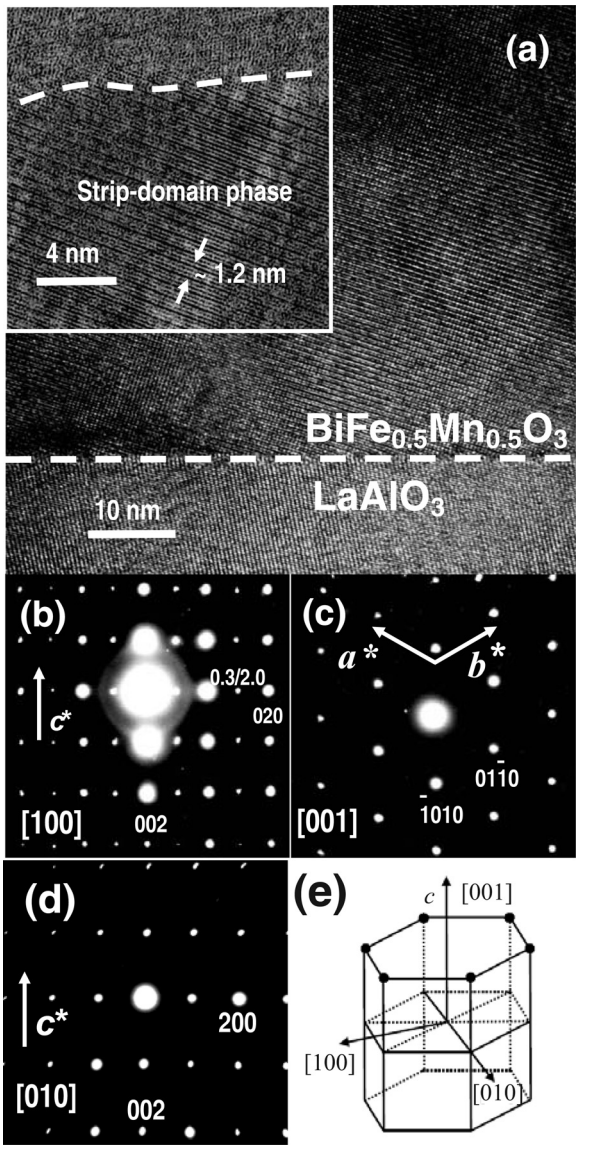

FIG. 2. (a) Low-magnification cross-sectional HREM image for the BFMO film. The dashed line indicates the interface between the film and the substrate. The inset presents the high-magnification HREM image for the strip-domain phase. The dashed line indicates the phase boundary. (b, c, and d) Selected area electron diffraction patterns of the BFMO film along the [100], [001] and [010] zone axes, respectively, for the hexagonal symmetry, represented by (e).

case the fast Fourier transform (FFT) of the HREM image (see Fig. 1(c)) produces additional superlattice reflections with a wave vector $q = c^*/3$ (indicated by white arrows), where c^* is the c axis (for cubic symmetry) reciprocal to the lattice vector. Additional analysis of the HREM images reveals that the strip-domain phase has orthorhombic crystal symmetry similar to that of the major phase.

Figure 2(a) shows the cross-sectional HREM image for BFMO, including the film/substrate interface. It can be seen that the film exhibits an atomically clean and sharp interface without an amorphous intermediate layer or precipitations. At the same time, statistical SAED analysis reveals three typical ED patterns related to different orientations of the crystal lattice with respect to the direction of the electron beam. Figures 2(b)–2(d) correspond to SAED patterns along the [100], [001] and [010] zone axes, respectively, for the hexagonal symmetry represented by Fig. 2(d). Therefore, in addition to the predominant *c*-oriented crystal structure the film contains *a*- and *b*-oriented nanocrystallites. Therefore, according to microstructure analysis, the prepared BFMO film has hexagonal crystal structure with lattice parameters $a \simeq b \simeq 0.471$ nm, $c \simeq 0.392$ nm, and the angle between the *a* and *b* axes is $\gamma \simeq 120°$. Notice that crystal lattice of this compound is usually indexed as an orthorhombic cell (from x-ray diffraction analysis).[13,15] Moreover, similarly to the BMO film, small-size regions of the strip-domain phase with the $3c$-periodic spacing, represented by the inset in Fig. 2(a), have been observed as well.

4. Magnetic properties

Figure 3 shows in-plane FC and ZFC temperature dependences of the magnetic moment, $M(T)$, for the BMO film taken at different applied magnetic fields after the extraction of diamagnetic response from the substrate. The inset displays the temperature dependence of the inverse dc magnetic susceptibility (χ^{-1}) in dimensionless units taken at the same magnetic fields in the ZFC regime. Curie temperature $T_C \simeq 105$ K, estimated as a point where the $\chi^{-1}(T)$ curve starts to deviate from Curie–Weiss (CW) linear behavior (straight line), is coincident with the published results for the bulk compound.[8] On the other hand, $M(T)$ behavior at $T \leq T_C$ is more typical for a superparamagnetic (SPM) system than for a valid ferromagnet, exhibiting smooth exponential increase in the magnetic

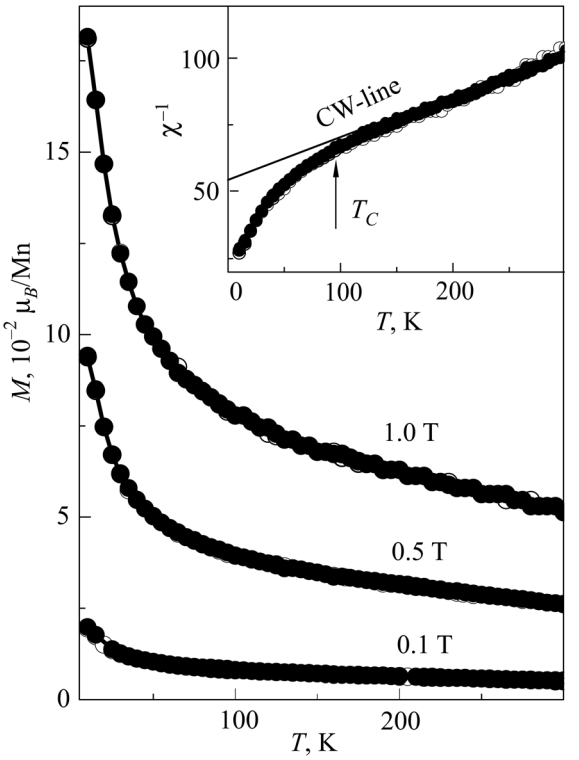

FIG. 3. Temperature dependence of the in-plane FC (solid symbols) and ZFC (open symbols) magnetic moment for the BMO film, measured at different applied magnetic fields. Lines serve as guides to the eyes. The inset presents the temperature dependence of the inverse dc magnetic susceptibility taken at the same applied fields in the ZFC regime. The solid line is the Curie–Weiss linear approximation. The arrow shows the onset of the FM transition.

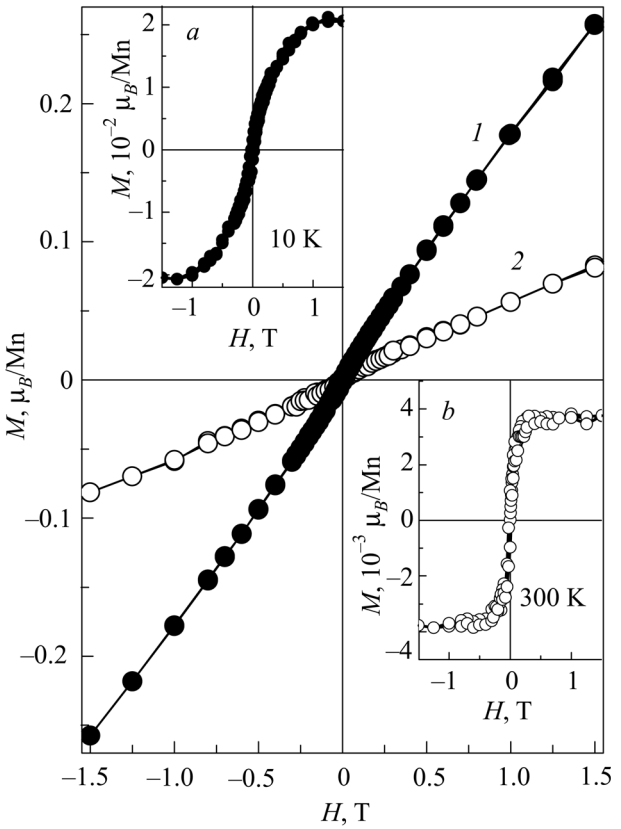

FIG. 4. In-plane magnetic hysteresis loops for the BMO film taken at $T = 10$ (*1*) and 300 (*2*) K. Lines serve as guides to the eyes. Insets *a* and *b* display in more detail the same dependencies after the extraction of the PM terms.

moment with decreasing temperature. Because $\chi^{-1}(T) \sim (T+\theta)/C_{CW}$ for PM materials,[22] where $C_{CW} = N(\mu_{\text{eff}})^2/3k_B$ is the CW constant obtained from the experimental curve, θ is a certain characteristic temperature, k_B is the Boltzmann constant, and N is the number of magnetic ions per unit cell; one can estimate the atom's effective magnetic moment in the PM phase, which turns out to be $\mu_{\text{eff}} \simeq 13\,\mu_B$. This value is larger than that predicted by the CW-theory for a classical PM, $\mu_{\text{eff}}^{\text{theor}} \simeq 4.9\,\mu_B$/Mn, using expression $\mu_{\text{eff}}^{\text{theor}} = g\sqrt{S(S+1)}$, where $g = 2$ is the Landé factor, and $S = 2$ for Mn^{3+}. A similar PM response with an enhanced magnetic moment has already been observed in manganites[23] and was attributed to the existence of small magnetic polarons typical for diluted magnetic semiconductors.

Figure 4 presents magnetic hysteresis loops, $M(H)$, for the BMO film at 10 and 300 K after the extraction of diamagnetic response from the substrate. Well-defined linear $M(H)$ dependences testify that a major part of the film is in the paramagnetic (PM) state at both temperatures with minor FM contributions (hysteresis terms with saturation). Insets *a* and *b* display the same dependencies after the extraction of PM terms in more detail. The hysteresis loops reveal a saturation magnetic moment $M_s \simeq 0.0044$ and $0.02\,\mu_B$/Mn, a remanent magnetic moment $M_r \simeq 0.001$ and $0.0016\,\mu_B$/Mn, and a coercive field $H_c \simeq 50$ and 350 Oe at 300 and 10 K, respectively. It is worth noting that a small FM response is observed at $T \gg T_C$, confirming the presence of small-size FM clusters in the PM matrix.

Figure 5 shows in-plane FC and ZFC temperature dependences of the magnetic moment, $M(T)$, taken at different applied magnetic fields for the BFMO film after the extraction of diamagnetic response from the substrate. The $M(T)$ behavior is very close to that observed for the BMO film. Linear extrapolation of the $\chi^{-1}(T)$ dependence, represented by the inset, reveals that $T_C \simeq 150$ K, which agrees with the published results.[9,10,16] The experimental value of $\mu_{\text{eff}} \simeq 12\,\mu_B$ in the PM phase is also larger than the theoretical one, $\mu_{\text{eff}}^{\text{theor}} \simeq 5.9\,\mu_B$/B-site ion. In this case the following expression was used: $\mu_{\text{eff}}^{\text{theor}} = g\sqrt{0.5S_1(S_1+1) + 0.5S_2(S_2+1)}$, where $S_1 = 2$ and $S_2 = 5/2$ for Mn^{3+} and Fe^{3+} ions, respectively.

Figure 6 presents magnetic hysteresis loops, $M(H)$, for the BFMO film at 10 and 300 K after the extraction of diamagnetic response from the substrate. Once again, similarly to BMO, the $M(H)$ behavior is typical for the multiphase magnetic system containing PM (linear term) and FM (hysteresis term with a saturation) contributions. Insets *a* and *b* display the same dependencies after the extraction of PM linear terms in more detail. The hysteresis loops reveal a saturation magnetic moment $M_s \simeq 0.01$ and $0.06\mu_B$/B-site ion, a remanent magnetic moment $M_r \simeq 0.002$ and $0.0075\mu_B$/B-site ion, and a coercive field $H_c \simeq 150$ and 400 Oe at 300 and 10 K, respectively. Small FM response is observed at room temperature ($T \gg T_C$) as well, verifying the existence of FM clusters with an enhanced magnetic moment in the PM matrix.

5. Discussion

The experimental data reveal that orthorhombic BMO and hexagonal BFMO films remain in the PM phase

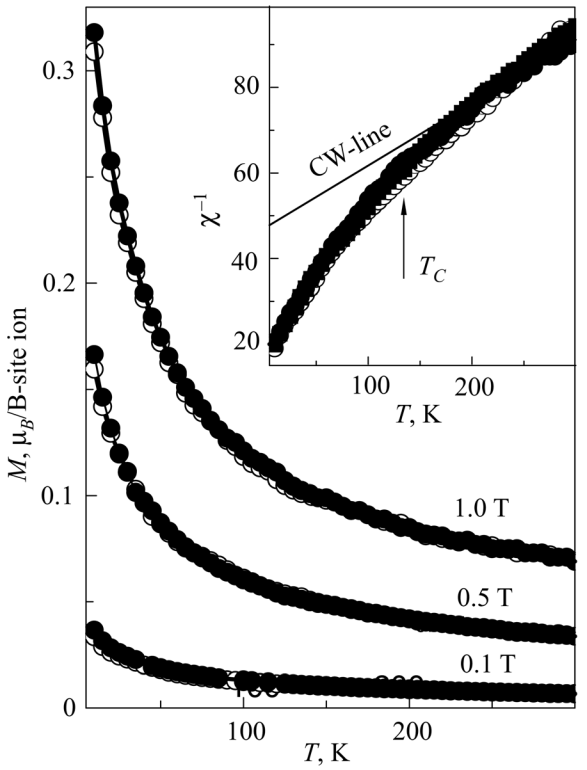

FIG. 5. Temperature dependence of the in-plane FC (solid symbols) and ZFC (open symbols) magnetic moments for the BFMO film, measured at different applied magnetic fields. Lines serve as guides to the eyes. The inset presents the temperature dependence of the inverse dc magnetic susceptibility taken at the same applied fields in the ZFC regime. The solid line is the Curie–Weiss linear approximation. The arrow defines the onset of the FM transition.

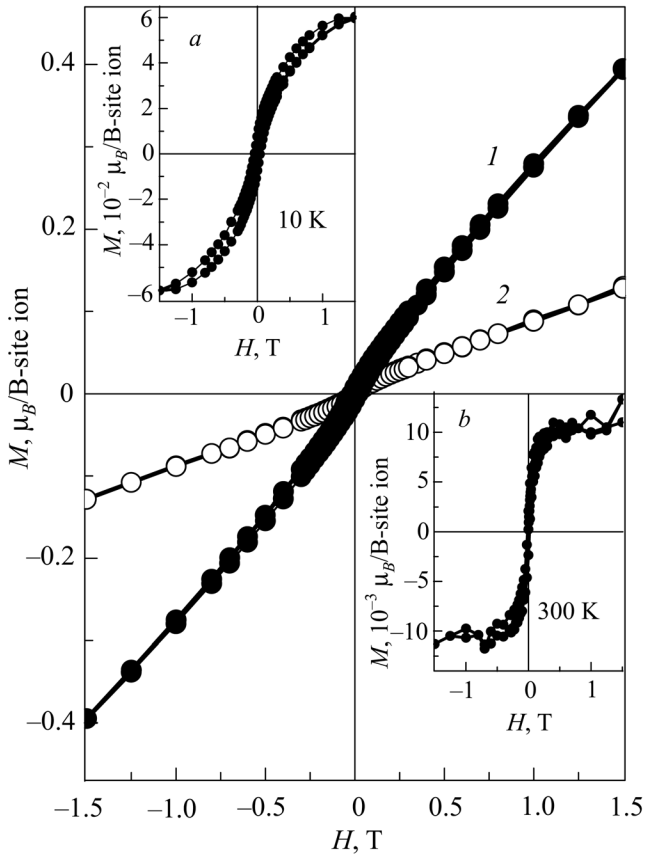

FIG. 6. In-plane magnetic hysteresis loops for the BFMO films taken at $T = 10$ (*1*) and 300 (*2*) K. Lines serve as guides to the eyes. Insets *a* and *b* display in more detail the same dependencies after the extraction of the PM terms.

throughout the entire investigated temperature interval. At the same time, the appearance of small FM response with nontypical for FMs $M(T)$ behavior deserves further discussion. Paramagnetic background of the films is confirmed by the lack of ZFC/FC $M(T)$ splitting at low temperature (see Figs. 3 and 5), but should be observed through exchange-bias interaction in the AFM matrix with FM entities.

In spite of the fact that the FM transition starts at 105 and 150 K in the BMO and BFMO films, respectively, complete long-range FM order is not observed even at the lowest temperature. Moreover, hysteresis loops with a saturation magnetic moment are observed at $T \gg T_C$ (insets *b* in Figs. 4 and 6). This kind of magnetic behavior is typical for the percolation system and should be considered within the context of the Griffiths-like model, which predicts the appearance of FM clusters in the temperature range $T_C(p_c) \le T \le T_G$, where $T_C(p_c)$ is the actual Curie temperature provided by the percolation threshold, and T_G is the highest achievable critical temperature.[24] In this case we deal with the first-order magnetic transition in which disorder has driven $T_C(p_c)$ to 0 K, and inverse susceptibility could be described by the power law: $\chi^{-1} \sim [T/T_C(p_c) - 1]^{1-y}$, where $y \le 1$.[25,26] Logarithmic plots, presented in the insets in Fig. 7, are a fit of the data to this power law with the result that $y = 0.66$ and 0.45, and $T_C(p_c) = 3$ and 1 K for the BMO and BFMO films, respectively. The obtained results agree with the theoretical predictions well and confirm the percolation origin of the FM transition in the investigated films. The Griffiths phase can be treated formally as an assembly of magnetic polaron clusters in diluted magnetic semiconductors[27] with the following temperature dependence of the magnetic moment: $M(T, H) = M(0, H)\exp(-k_BT/\mu_{\text{eff}}H)$, where $M(0, H)$ is the magnetic moment at $T = 0$ K, and μ_{eff} is the effective magnetic moment of the magnetic polaron cluster. Therefore, the total value of magnetic susceptibility for BMO and BFMO films can be expressed by $\chi(T, H) = \chi_0^G \exp(-k_BT/\mu_{\text{eff}}H) + C_{CW}/(T + \theta)$, where $\chi^G{}_0$ is susceptibility of the Griffiths phase at $T = 0$ K. The first term belongs to the FM clusters (Griffiths phase), while the second one corresponds to the major PM part of the sample. Figure 7 shows ZFC $\chi(T)$ dependences for BMO and BFMO films taken at different values of applied magnetic field: $H = 0.1$ (solid circle), 0.5 (open circle), and 1.0 T (solid square). Solid lines are the theoretical curves constructed with fitting parameters $\chi_0^G = 0.028$ and 0.03 in dimensionless units, and $\mu_{\text{eff}} = 350$ and $450\,\mu_B$ for BMO and BFMO, respectively. The PM term was obtained from the linear extrapolation of the $\chi^{-1}(T)$ experimental curves, represented by the insets in Figs. 3 and 5. It is seen that the theoretical curves agree with the experimental ones very well. Because the theoretical average magnetic moment for BMO and BFMO, respectively, is 4.9 and $5.4\,\mu_B$/B-site ion, the estimated average diameter of a magnetic polaron cluster in the Griffiths phase turns out to be $D \simeq 2$ nm.

In spite of the fact that measured films have different crystal lattices—orthorhombic and hexagonal—the same microstructure peculiarity is observed in both cases. There is a strip-domain phase with periodic spacing of about $3c$. We

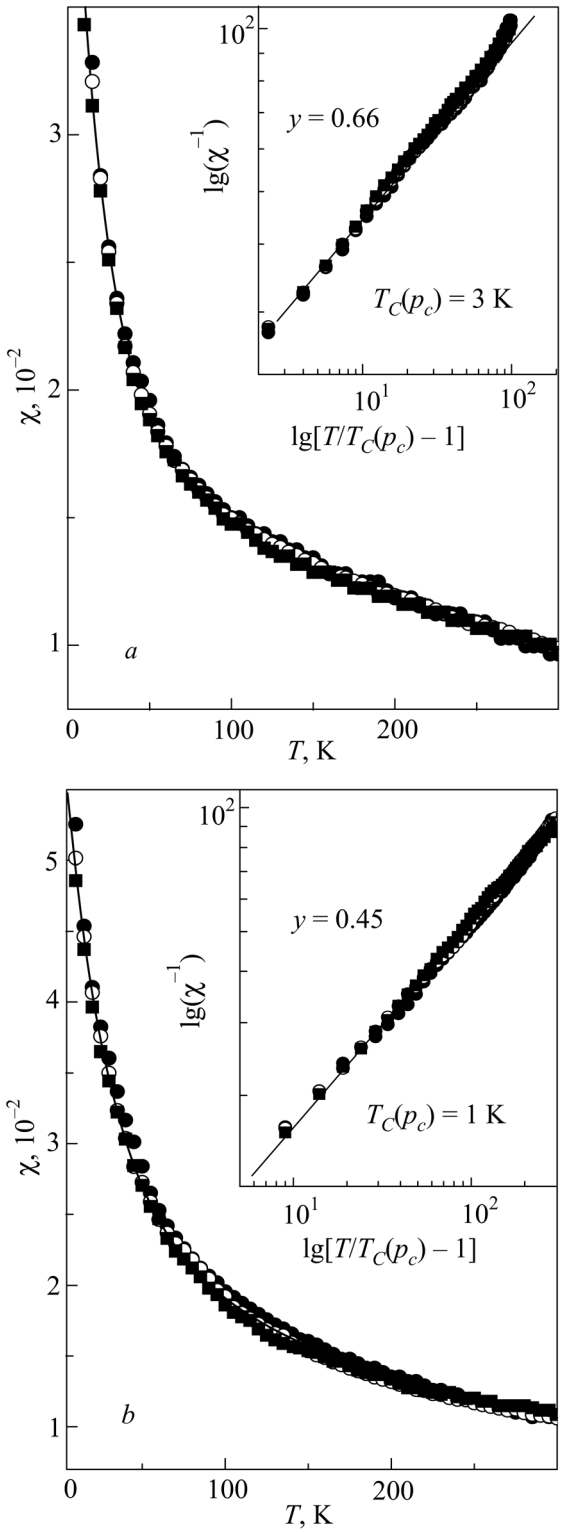

FIG. 7. Temperature dependence of the in-plane ZFC magnetic susceptibility for the BMO (a) and BFMO (b) films, measured at different applied magnetic fields. The solid line is the theoretical curve obtained within the framework of the Griffiths-phase model. The inset presents the logarithmic plot of inverse susceptibility vs. normalized temperature. The solid straight line is a fit of the experimental data to the percolation power law, discussed in the text.

argue that this low-dimensional layered structure is the origin of weak ferromagnetism in the BMO and BFMO films, acting through the formation of the Griffiths-phase state. It should be noted that a similar phenomenon has already been observed in hole-doped manganite films, where the appearance of long periodic strip-domain structure is attributed to specific ordering between rare-earth and doped ions.[28,29]

However, in our case the strip-domain phase is rather governed by the cooperative Jahn–Teller effect since Mn^{3+} and Fe^{3+} belong to the so-called Jahn–Teller-type ions and tend to orbital ordering and charge.[30]

Conclusions

In summary, the $BiMnO_3$ and $BiFe_{0.5}Mn_{0.5}O_3$ films were prepared by rf magnetron sputtering on a $LaAlO_3$ (001) single-crystalline substrate. The selected-area electron diffraction analysis allowed us to identify the crystal structure of the $BiMnO_3$ film as orthorhombic, and the $BiFe_{0.5}Mn_{0.5}O_3$ film as having hexagonal lattice symmetry. High-resolution electron-microscopy study revealed the presence of the strip-domain phase with a periodic spacing of about $3c$ in both films. Magnetic measurements showed that in addition to the basic paramagnetic phase the films exhibit Griffiths phase behavior in a wide temperature range. Therefore, weak ferromagnetism observed in the $BiMnO_3$ and $BiFe_{0.5}Mn_{0.5}O_3$ films is provided by the appearance of the strip-domain layered phase, rather than an intrinsic physical origin.

This work was supported by the NRF/MEST through the Quantum Photonic Science Research Center, Korea. V. Svetchnikov is grateful for the financial support of the Netherlands Institute for Metal Research.

[a)]Email: pvg@imp.kiev.ua

[1]X. Qi, J. Dho, R. Tomov, M. G. Blamire, and J. L. MacManus-Driscoll, Appl. Phys. Lett. **86**, 062903 (2005).
[2]W. Eerenstein, F. D. Morrison, J. Dho, M. G. Blamire, J. F. Scott, and N. D. Mathur, Science **307**, 1203a (2005).
[3]N. A. Spaldin and M. Fiebig, Science **309**, 391 (2005).
[4]V. G. Prokhorov, G. G. Kaminsky, J. M. Kim, T. W. Eom, J. S. Park, Y. P. Lee, V. L. Svetchnikov, G. G. Levtchenko, Yu. M. Nikolaenko, and V. A. Khokhlov, Fiz. Nizk. Temp. **37**, 161 (2011) [Low Temp. Phys. **37**, 129 (2011)].
[5]C. Ederer and N. Spaldin, Phys. Rev. B **71**, 060401 (2005).
[6]I. Dzyaloshinskii, J. Phys. Chem. Solids **4**, 241 (1958).
[7]T. Moria, Phys. Rev. **120**, 91 (1960).
[8]F. Sugawara, S. Iida, Y. Syono, and S. Akimoto, J. Phys. Soc. Jpn. **20**, 1529 (1965).
[9]A. F. Moreira dos Santos, S. Parashar, A. R. Raju, Y. S. Zhao, A. K. Cheetham, and C. N. R. Rao, Solid State Commun. **122**, 49 (2002).
[10]A. F. Moreira dos Santos, A. K. Cheetham, W. Tian, X. Pan, Y. Jia, N. J. Murphy, J. Lettieri, and D. Schlom, Appl. Phys. Lett. **84**, 91 (2004).
[11]Z. H. Chi, H. Yang, S. M. Feng, F. Y. Li, R. C. Yu, and C. Q. Jin, J. Magn. Magn. Mater. **310**, 358 (2007).
[12]T. Shishidou, N. Mikamo, Y. Uratani, F. Ishii, and T. Oguchi, J. Phys.: Condens. Matter **16**, S5677 (2004).
[13]M. Azuma, H. Kanda, A. A. Belik, Y. Shimakawa, and M. Takano, J. Magn. Magn. Mater. **310**, 1177 (2007).
[14]L. Bi, A. R. Taussing, H. S. Kim, L. Wang, G. F. Dionne, D. Bono, K. Persson, G. Ceder, and C. A. Ross, Phys. Rev. B **78**, 104106 (2008).
[15]P. Mandal, A. Sundaresan, C. N. R. Rao, A. Iyo, P. M. Shirage, Y. Tanaka, Ch. Simon, V. Pralong, O. I. Lebedev, V. Caignaert, and B. Raveau, Phys. Rev. B **82**, 100416 R (2010).
[16]Y. Du, Z. X. Cheng, S. X. Dou, X. L. Wang, H. Y. Zhao, and H. Kimura, Appl. Phys. Lett. **97**, 122502 (2010).
[17]E. M. Choi, S. Patnaik, S.-L. Sahonta, H. Wang, Z. Bi, J. Xiong, M. G. Bamire, Q. X. Jia, and J. L. MacManus-Driscoll, Appl. Phys. Lett. **98**, 012509 (2011).
[18]J. Miao, X. Zhang, Q. Zhan, Y. Jiang, and K.-H. Chew, Appl. Phys. Lett. **99**, 062905 (2011).
[19]V. N. Varyukhin, Yu. V. Medvedev, Yu. M. Nikolaenko, A. B. Mukhin, B. V. Belyaev, V. A. Gritskikh, I. V. Zhikharev, S. V. Kara-Murza, N. V. Korchikova, and A. A. Tikhii, Tech. Phys. Lett. **35**, 937 (2009).

[20]H. Yang, Z. H. Chi, J. L. Jiang, W. J. Feng, Z. E. Cao, T. Xian, C. Q. Jin, and R. C. Yu, J. Alloys Compd. **461**, 1 (2008).
[21]A. A. Belik, K. Kodama, N. Igawa, S. Shamoto, K. Kosuda, and E. Takayama-Muramachi, J. Am. Chem. Soc. **132**, 8137 (2010).
[22]B. D. Cullity, *Introduction to Magnetic Materials* (Addison-Wesley, New York, 1972).
[23]J. A. Souza, J. J. Neumeier, and Y. K. Yu, Phys. Rev. B **78**, 014436 (2008).
[24]R. B. Griffiths, Phys. Rev. Lett. **23**, 17 (1969).
[25]A. J. Bray, Phys. Rev. Lett. **59**, 586 (1987).
[26]A. H. Castro Neto, G. Castilla, and B. A. Jones, Phys. Rev. Lett. **81**, 3531 (1998).
[27]V. M. Galitski, A. Kaminski, and S. D. Sarma, Phys. Rev. Lett. **92**, 177203 (2004).
[28]Y. H. Hyun, J. S. Park, T. W. Eom, G. H. Kim, Y. S. Lee, Y. P. Lee, V. G. Prokhorov, and V. L. Svetchnikov, Appl. Phys. Lett. **93**, 042515 (2008).
[29]T. W. Eom, Y. H. Hyun, J. S. Park, Y. P. Lee, V. G. Prokhorov, V. S. Flis, and V. L. Svetchnikov, Appl. Phys. Lett. **94**, 152502 (2009).
[30]M. J. Calderón, A. J. Millis, and K. H. Ahn, Phys. Rev. B **68**, 100401(R) (2003).

This article was published in English in the original Russian journal. Reproduced here with stylistic changes by AIP.